ACS APPLIED NANO MATERIALS

www.acsanm.org Article

Hydrogen-Mediated CVD Epitaxy of Graphene on SiC: Implications for Microelectronic Applications

Zouhour Ben Jabra, Isabelle Berbezier,* Adrien Michon, Mathieu Koudia, Elie Assaf, Antoine Ronda, Paola Castrucci, Maurizio De Crescenzi, Holger Vach, and Mathieu Abel

Cite This: *ACS Appl. Nano Mater.* 2021, 4, 4462−4473 Read Online

ACCESS | Metrics & More | Article Recommendations | Supporting Information

ABSTRACT: Despite the large body of literature reporting on the growth of graphene (Gr) on 6H−SiC(0001) by chemical vapor deposition (CVD), some important issues have not yet been solved, and full-wafer-scale epitaxy of Gr remains challenging, hampering applications in microelectronics. With this study, we shed light on the generic mechanism which produces the coexistence of two different types of Gr domains: Gr on hydrogen (H-Gr) and Gr on buffer layer ((6 × 6) Gr), whose proportion can be carefully controlled by tuning the H_2 flow rate. We show for the first time that the growth of Gr by CVD under a H_2/Ar flow rate proceeds in two stages. First, the nucleation of free-standing epitaxial Gr on hydrogen (H-Gr) occurs; then, H-atoms eventually desorb from either step edges or defects. This gives rise, for a H_2 flow rate below a critical value, to the formation of (6 × 6) Gr domains. The front of H-desorption progresses proportionally to the reduction of H_2. Using the robust and generic X-ray photoelectron spectroscopy (XPS) analysis, we realistically quantify the proportions of H-Gr and (6 × 6) Gr domains of a Gr film synthesized under any experimental conditions. Scanning tunneling microscopy supports the XPS measurements. From these results, we can deduce that the H-assisted CVD growth of Gr developed here is a unique method to grow fully free-standing H-Gr in contrast to the method consisting of H-intercalation below (6 × 6) Gr epitaxial layer. These results are of crucial importance for future applications of Gr/SiC(0001) in nano- and microelectronics and in particular for field-effect transistors, for which maximization of mobility is mandatory. This work also provides the groundwork for the use of Gr as an optimal template layer for van der Waals homo- and heteroepitaxy for optoelectronic applications.

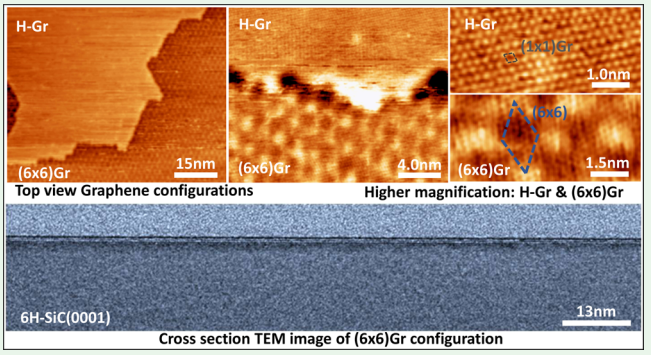

KEYWORDS: *graphene, 6H−SiC, CVD, STM, growth mechanism, atomic configuration, structural properties*

INTRODUCTION

Since 2004, the unique properties of graphene (Gr), a single layer of graphite,[1−4] have attracted a substantial research interest.[5] Instead of graphite presenting a parabolic dispersion at the K-point of the Brillouin zone,[6] Gr has a planar honeycomb structure and a linear dispersion.[2,7] Electrons behave like massless fermions around the Fermi energy level with an unprecedented Fermi velocity.[8,9] Gr was initially obtained by exfoliation from bulk graphite[8] and then transferred onto silicon oxide.[4] This procedure suffers from important electron−phonon scattering at the interface between Gr and the substrate underneath, resulting in carrier mobility reduction.[10] Alternative substrates were then efficiently explored for the catalytic growth of Gr such as metals (Ni,[11] Pt,[12] Ru,[13] Pd,[14] Cu[15]), III−V alloys,[16] and boron nitride (h-BN),[17] proving that high-quality Gr can be properly transferred on various substrates. However, even if the exfoliation technique is simple, inexpensive, and perfectly fitted to fundamental physics, its technological development is not enough when it comes to applications (in particular, for the microelectronic industry).[18] This is because Gr flakes are not large (and homogeneous) enough despite the efforts being devoted to improving the process for large-scale applications.[3,19,20]

The growth of Gr by the sublimation process (called graphitization)[21,22] was then considered as a technique of choice for potential industrial applications. It is achieved by thermal decomposition of SiC substrates at temperatures around 1600−2000 °C under ultra-high vacuum (UHV)[23,24] or under an Ar atmosphere.[21,25] The method consists of sublimating silicon atoms from the SiC substrate, leaving behind carbon atoms in a Gr-like layer. About 30% of these carbon atoms are covalently bound to the Si ones underneath

Received: January 11, 2021
Accepted: April 22, 2021
Published: May 10, 2021

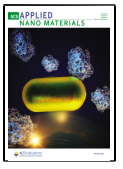

https://doi.org/10.1021/acsanm.1c00082
ACS Appl. Nano Mater. 2021, 4, 4462−4473

at the origin of the $(6\sqrt{3} \times 6\sqrt{3})$R30° reconstructed interface layer called the buffer or zero layer, [hereafter referred to as (6 × 6)]. However, thermal decomposition is not self-limiting, and Gr films produced on both Si(0001)- and C(000−1)-terminated surfaces are commonly composed of few submicrometer domains with 1−3 ML thickness. Uniformity on full-scale wafers remains challenging. Gr grows much faster on the C- face and forms larger domains (~200 nm) of multilayer-rotated Gr films (resulting from morphological changes of the SiC surface during Si sublimation) than on the Si-face, where domains have a size of less than 100 nm but single orientation.[26] In order to obtain Gr layers with more uniform thickness, various approaches have been proposed to counteract the Si sublimation rate, for example, using simultaneous Si deposition (or using a mixture of Si and N_2). The idea is to approach the thermodynamic equilibrium and better control the C-rich $(6\sqrt{3} \times 6\sqrt{3})$ R30° buffer layer and the resulting Gr thickness.[27,28] Employing high-pressure Ar was also reported as an efficient way to reduce the Si evaporation since part of the desorbed Si atoms are reflected back to the surface by collision with Ar atoms.[21,29] A high sublimation temperature was also shown to restructure and uniformize the terrace morphology.

Since only H-Gr (free-standing) is supposed to have high-carrier mobility and relevant electronic properties, recent approaches have been developed to decouple the Gr layer from the substrate by H intercalation,[30] that is, by passivating the dangling bonds of Si atoms at the SiC interface.[30] However, this H intercalation process, starting from (6 × 6) Gr epitaxial layers, does not produce full H-Gr layers [as testified by the presence of weak spots representative of the $(6\sqrt{3} \times 6\sqrt{3})$ R30° buffer layer on low energy electron diffraction (LEED) patterns].[30] Decoupling the Gr/metal substrate interface was also performed by metals intercalation, such as Co,[31] Fe,[32] Au,[33] Pb,[34] oxygen,[35] and hydrogen.[36] However, Gr decoupled by metals is not suitable for applications in microelectronics and would require film transfer onto insulating substrates, procedure leading to defect creation.

The consequence of Gr inhomogeneity is to induce low-carrier mobility and current on/off (I_{on}/I_{off}) ratios typically in the order of 10 in a conventional design.[37] This number should be increased using higher quality Gr and higher gating efficiency. On the other hand, for digital transistors used in logic applications, on/off current ratios higher than $\sim 10^4$ are required according to International Technology Roadmap for Semiconductors. This can only be achieved if a large-scale homogeneous well-controlled single monolayer (ML) Gr is used for the fabrication of transistors. It is only in a second step that much research effort could be spent at opening a band gap in these Gr layers.

More recently, Gr has also been grown using a carbon source[38] either by UHV-molecular beam epitaxy[38] or by chemical vapor deposition (CVD) under an Ar[39,40] or H_2 atmosphere[41] to meet the requirements of technological applications. SiC, the first naturally used substrate, has many advantages for the direct growth of Gr,[22] in particular, for providing reproducible and reliable high-quality Gr layers with a well-controlled and homogeneous thickness on a large scale[42] both on Si- and C- faces of SiC(0001). It was reported[39,43] that depending on the growth temperature and carrier gas pressure, Gr can be grown on top of the buffer layer [henceforth, referred to as (6 × 6) Gr] that has the $(6\sqrt{3} \times 6\sqrt{3})$ R30° superstructure resulting from covalent bonds with the SiC substrate. The (6 × 6) Gr obtained by CVD on top of the buffer layer reconstructed $(6\sqrt{3} \times 6\sqrt{3})$R30° has a structure very similar to the one of epitaxial Gr obtained by graphitization which has been extensively studied.[39,40] On the other hand, the H-Gr configuration was only reported as the result of the intercalation of H_2 below the epitaxial (6 × 6) Gr using a H_2 flux at temperatures below 900 °C to avoid H_2 desorption,[30,44,45] while its formation by CVD using a C-based gas (i.e. propane) and the H_2 (or H_2/Ar mixtures) carrier gas has already been demonstrated by Michon et al.[41,42]

In this work, we report the atomic configurations of Gr layers grown by CVD on 6H−SiC (0001) terminated Si, for three different (H_2/Ar) carrier gas ratios, and we deduce new insights into the Gr growth mechanisms. Atomic force microscopy (AFM), scanning tunneling microscopy (STM), LEED, and X-ray photoelectron spectroscopy (XPS) analyses give evidence for different structural characteristics of the surfaces depending on the CVD conditions. For the first time, we demonstrate that the complex interplay between growth and etching mechanisms at work in the close to equilibrium conditions used can produce full coverage of H-Gr or of (6 × 6) Gr depending on the H_2/Ar flux ratio, the transition between the two configurations being controlled only by hydrogen desorption. More precisely, we have found that for a H_2/Ar ratio of 9%, only (6 × 6) Gr grows. At increasing H_2/Ar ratios, we observe the coexistence H-Gr and (6 × 6) Gr domains, and finally, at a 42% ratio, a full H-Gr layer is obtained. The amount of H-Gr and the percentage of coexistence of (6 × 6) Gr and H-Gr domains have been assessed by XPS, STM, and LEED careful analyses. These investigations indicate that the switch between these two configurations is controlled by hydrogen desorption. The presence of juxtaposed areas of (6 × 6) Gr and H-Gr, which is underestimated in many studies, has a great influence on the subsequent deposition of van der Waals heterostructures.[46−48] It also has strong effects in terms of electrical properties since the buffer layer is not equivalent to Gr. It is not conducting because of the sp^3 bonding to the SiC substrate and it is also responsible for the n-type doping of Gr due to the presence of unsaturated Si bonds. Usually, the reported values of both the electron mean free path and the carrier mobility in Gr on SiC are significantly lower than those in suspended Gr. For instance, the electron-mean-free path in Gr on SiC is about 40% lower than those of suspended Gr, and it also exhibits large variations from point to point, due to the presence of a laterally inhomogeneous positively charged layer at the Gr/SiC interface.[49−51] In addition, our results show that CVD is a unique technique to grow uniform and homogeneous H-Gr MLs at a full-wafer scale and with very low density of defects that can serve as robust pseudosubstrates for van der Waal heteroepitaxy. The use of such uniform Gr layers is also mandatory for the fabrication of reliable microelectronic devices such as field-effect transistors.

RESULTS AND DISCUSSION

As reported in the Experimental Section, we performed several H_2/Ar ratio CVD growths on the 6H−SiC(0001) substrate. A simplified schematic representation of the CVD process is given in Figure 1.

For all the obtained samples, the AFM images always present the same features as shown in Figure 2 (the image corresponds to sample A where Gr is obtained at 1550 °C, during 15 min with 9% of H_2): large flat terraces with mean

https://doi.org/10.1021/acsanm.1c00082
ACS Appl. Nano Mater. 2021, 4, 4462−4473

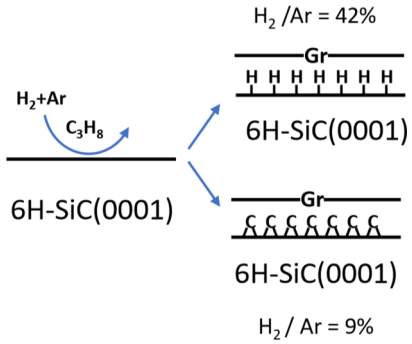

Figure 1. Schematic representation of the CVD growth process at high- and low-H_2 flows.

widths between 200 nm and 1 μm (Figure 2a), separated by multilayer steps (see line profile in Figure 2b). Their height is commonly around 0.75 nm corresponding to tri-layer SiC steps; a few higher ones are also observed with a height of ≈1.5 nm which corresponds to the total SiC crystalline cell (c = 1.51 nm). Some narrower terraces, separated from the larger ones by monoatomic SiC steps (Figure 2c and corresponding line profile in Figure 2d), with 0.25 nm mean height corresponding to single SiC ML are also observed. These step heights have already been observed along the ⟨1000⟩ direction of 6H−SiC.[38,52] All these morphological features prove the preservation of the initial topography of the substrate.

The Gr thin film having a carpet-like morphology completely covers the SiC surface and then cannot be observed at the AFM scale. In the case of a full (6 × 6) Gr or full H-Gr, there are no changes of the height difference between two neighbor terraces. In the case of coexisting domains, height differences are too small to be visible by AFM [height difference between (6 × 6) Gr and H-Gr is expected to be 0.154 nm]. Few specific irregular step edges and rough terraces morphologies observed on the surface (Figure 2c) are also assigned to the bare SiC substrate underneath. In order to obtain only one ML Gr growth, it is fundamental to suitably dose the percentage of the hydrogen, argon, and propane gases. Indeed, the surface morphology strongly depends on the competition between H_2 etching of the SiC surface and C_3H_8-promoting Gr growth:[53,54] small additions of propane to the hydrogen atmosphere suppress the etching of SiC, while too large quantities could degrade the surface morphology.[53] Our CVD experimental conditions are very close to the thermodynamic equilibrium ones. This ensures the formation of only one ML of Gr, whatever the growth duration. The Gr growth rate mainly depends on the H_2 flow rate while temperature and total pressure only have minor effects. Moreover, the introduction of C_3H_8 is carefully controlled to avoid any morphological damage.

Atomic structural properties of epitaxial Gr grown on clean 6H−SiC(0001) are investigated by STM observations and LEED and XPS analyses.

Systematic investigation of the Gr films was performed on the as-grown samples and after annealing. The detailed analysis of three typical samples obtained in different experimental conditions is reported. The first Gr film was obtained in low H_2 flux (sample A in Table 1 given in Experimental Section). In this condition, the presence of H_2 under the Gr film is very

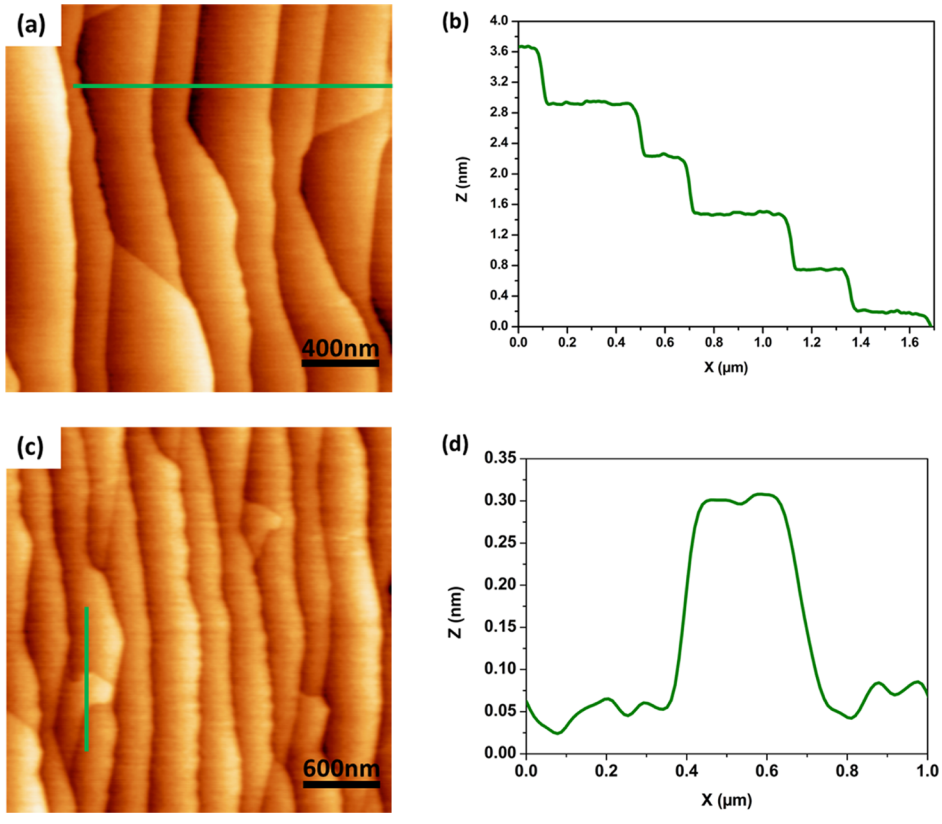

Figure 2. Gr epitaxially grown on 6H−SiC(0001) with 9% H_2 (sample A). (a) 2 × 2 μm2 AFM image of the Gr/SiC train of steps and terraces. (b) Typical line profile of the surface. (c) AFM image of an area with a narrower terrace separated by ML SiC steps (0.25 nm height). (d) The corresponding line profile. The z scale for both images is 0−1.6 nm.

https://doi.org/10.1021/acsanm.1c00082
ACS Appl. Nano Mater. 2021, 4, 4462−4473

Table 1. Growth Parameters Used for the Samples Studied in This Work[a]

sample	t (min)	% H_2	T (°C)	C_3H_8 (sccm) %	Gr/substrate interactions
A	15	9	1550	0.08	Gr on buffer layer
B	5	33	1600	0.04	Gr partly hydrogenated
C	5	42	1550	0.04	Gr fully hydrogenated

[a]All the samples were prepared under the same pressure (800 mbar). The last column gives information on the Gr/substrate interface.

unlikely. Large-scale STM images show a train of steps similar to the one observed by AFM separated by steps with heights of about 0.75 nm (Figure 3a). Atomic resolution STM images

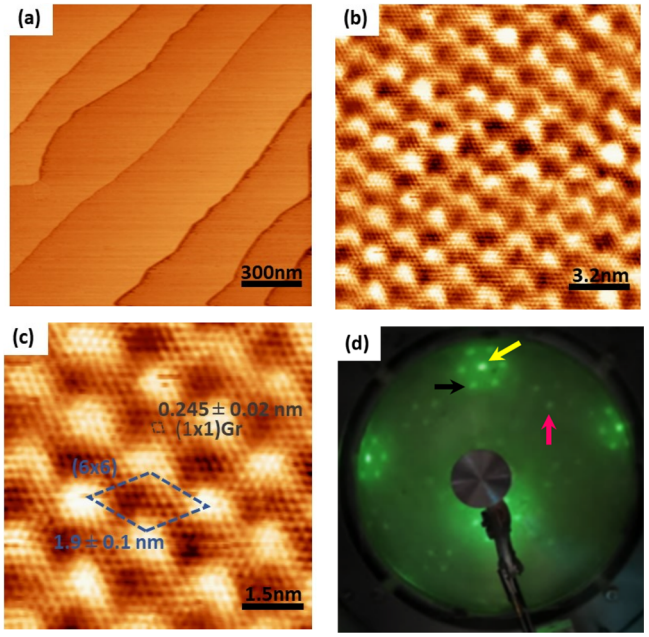

Figure 3. (a) Large-scale STM image showing the train of SiC steps under the Gr surface grown with a H_2 ratio of 9% (sample A). (b) STM atomic resolution image of the (6 × 6) and (1 × 1) Gr superimposed lattices. (c) Higher magnification image of the Gr atomic cell. (d) Corresponding LEED pattern: pink, yellow, and black arrows indicate (1 × 1) SiC, (1 × 1) Gr, and ($6\sqrt{3} \times 6\sqrt{3}$) Gr, respectively ($E$ = 35 eV). Tunneling parameters: (a) I_t = 0.495 nA and U_{bias} = −0.412 V; (b) and (c) I_t = 0.56 nA and U_{bias} = −1.56 V.

reveal two superimposed honeycomb lattices having periodicities of 3.2 ± 0.1 nm and 0.245 ± 0.02 nm that are ascribed to the ($6\sqrt{3} \times 6\sqrt{3}$) R30° 6H−SiC supercell[a] and to Gr lattice parameter, respectively (Figure 3b). The (6 × 6) reconstruction has a corrugation height around 0.03 nm which is assigned to the partial interfacial interaction between the C atoms of the first deposited layer (buffer layer) and the Si atom-terminated 6H−SiC(0001).

The superimposition of the two lattices (6 × 6) SiC and (1 × 1) Gr can be better appreciated on a higher magnification STM image (Figure 3c). This feature which has been systematically observed all over the surface of this sample testifies that the buffer layer covers the whole surface. Such STM images have been already reported for epitaxial Gr obtained by sublimation of 6H−SiC(0001)[55] and of 4H−SiC(0001).[44] The main difference is the smoothness and uniformity of the surface which are better under our CVD experimental growth conditions.

The presence of the buffer layer is also confirmed by the LEED pattern (Figure 3d). It reveals spots being the signature of the (1 × 1) SiC hexagonal lattice (indicated by the pink arrow) of the (1 × 1) Gr honeycomb network rotated by 30° with respect to SiC one (indicated by the yellow arrow) and higher intensity spots (highlighted by the black arrow) located at vertexes of hexagons and positioned around the Gr spots that are representative of the ($6\sqrt{3} \times 6\sqrt{3}$) R30° reconstruction. Such patterns have been already reported widely in the literature for Gr grown on the buffer layer.[24,56,57] These superstructure spots correspond to the periodicity of the buckling of the buffer layer induced by its strong covalent interaction with the terminating Si-atoms of the SiC substrate, as observed by STM.[58−60]

XPS spectra of C 1s (Figure 4a) and Si 2p (Figure 4b) recorded on the same sample have been fitted and analyzed after extraction of the background. The C 1s peak was deconvoluted assuming that four components are already identified in the literature:[61] (I) C−Si bonds of the SiC bulk substrate (corresponding to C in sp^3 configuration); (II) the top Gr layer (corresponding to C in the sp^2 hybridization); (III) the buffer layer which shares covalent bonds with the substrate; (IV) the buffer layer in sp^2 configuration (no bonds with the substrate). The two last contributions, named S1 and S2, have been well detailed in ref 61, and their ratio (S1/S2 integrated area ratio) was estimated around 0.5.[24,61] Under these experimental conditions, the best fit of the C 1s peak is obtained when four components of the pure (6 × 6) Gr (see Supporting Information S1 for details of the procedure) are located at E_{SiC} = 283.4 eV, E_{Gr} = 284.2 eV, E_{S1} = 284.6 eV, and E_{S2} = 285.3 eV in very good agreement with literature data. The results are consistent with a sample fully covered with (6 × 6) Gr.

Another important issue is the number of deposited (6 × 6) Gr layers deposited which is a key factor for applications. This quantity is estimated by the quantification of the C 1s/Si 2p area ratio, which is found around 1.55 for this sample. Such a ratio excludes the possibility for having more than 1 ML and then refers to a single (6 × 6) Gr ML. In addition, it confirms the presence of one (6 × 6) Gr ML in agreement with STM observation which shows evidence for a corrugation of about 0.03 nm corresponding, to the first free-standing (6 × 6) Gr layer according to the literature.[57,62] Indeed, by increasing the number of Gr layers, the measured corrugation is expected to lower.[58,63] The high resolution transmission electron microscopy (TEM) cross-section image of the sample (Figure 4c) shows evidence for the buffer layer and the top (6 × 6) Gr at the interplanar distances already reported in the literature. Therefore, all these results confirm that in these experimental conditions with a low H_2 flow rate, a high-quality ML of (6 × 6) Gr is formed in perfect epitaxy with the SiC substrate. The film has few defects and very good homogeneity and uniformity throughout the full-scale sample as testified by large-scale TEM cross-section images of the (6 × 6) Gr layer (see Supporting Information S2).

The second investigated Gr film was obtained with a large H_2 ratio of ∼42% (sample C in Table 1). The surface structure observed by STM exhibits a regular train of steps with no visible difference on the large-scale image with the previous sample. However, the atomic resolution images reveal the presence of only one honeycomb structure with a 0.245 nm lattice parameter (Figure 5b) which corresponds to the free-standing Gr layer (named H-Gr here). This suggests that in

https://doi.org/10.1021/acsanm.1c00082
ACS Appl. Nano Mater. 2021, 4, 4462−4473

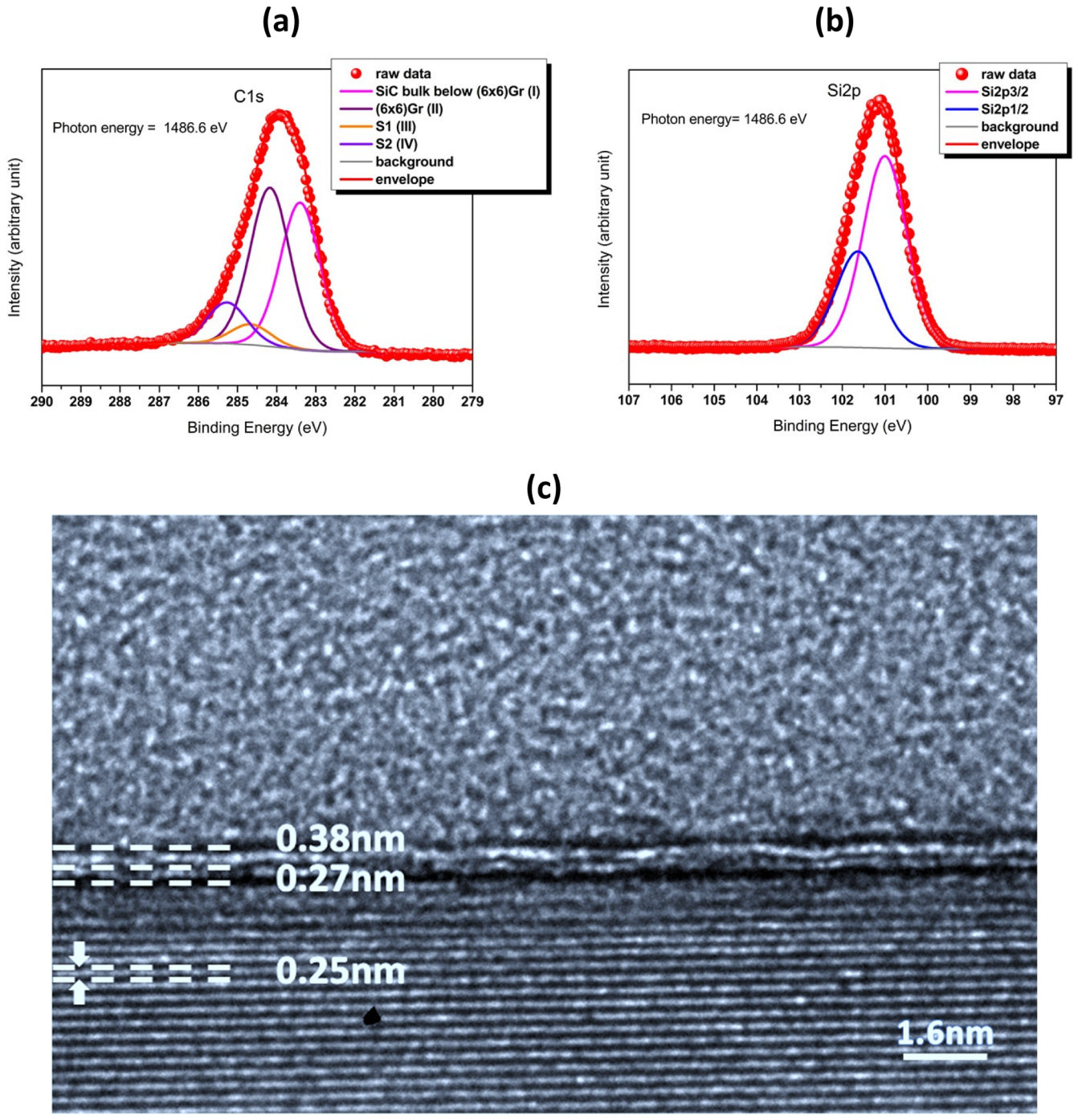

Figure 4. (a) C 1s and (b) Si 2p core level XPS spectra of Gr grown with H_2 = 9% (sample A) and their deconvolution into different carbon and silicon components, respectively. The different fitted components (solid lines) are labeled in both spectra. The solid red circles refer to the experimental data. (c) High-resolution TEM (HRTEM) cross-sectional image of the corresponding sample.

this sample, H is located under the Gr layer interface and saturates the Si dangling bonds as already observed in the literature.[30,44,61,64] Most of the H-Gr layers reported in the literature have been obtained by postgrowth hydrogenation of (6 × 6) Gr, that is, intercalation of H between the (6 × 6) buffer layer and the SiC substrate. In these experiments, the buffer layer transforms into a second Gr layer beneath the initial top (6 × 6) Gr layer. The H diffusion channels pass through step edges and surface crystalline defects. Hydrogenation is commonly incomplete as testified by the (6 × 6) reconstruction spots always observed on the LEED patterns.[30,44] In our experimental conditions, the complete sample is instead hydrogenated. Indeed, STM measurements do not display any area with (6 × 6) Gr (Figure 5a) and at higher magnification (Figure 5b), STM images show the uniform intensity of all the atoms of the (1 × 1) Gr honeycomb network. This is typical of free-standing H-Gr and in stark contrast with graphite where only half of the atoms of the hexagon are visible (triangular cell). Indeed, in graphite, the carbon planes are stacked according to the Bernal arrangement, where the second C plane shifted with respect to the first induces half of the atoms that are aligned vertically

https://doi.org/10.1021/acsanm.1c00082
ACS Appl. Nano Mater. 2021, 4, 4462−4473

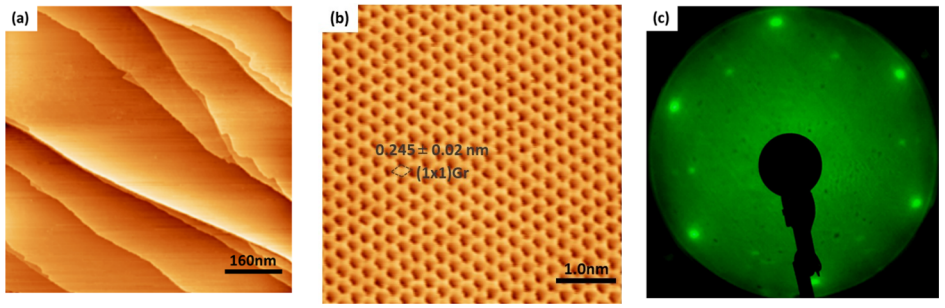

Figure 5. (a) Large-scale STM image of Gr grown with H_2 = 42% (sample C) (scanned areas: 800 × 800 nm2). (b) Higher magnification STM image of (a) showing evidence for the (1 × 1) Gr crystalline cell. (c) LEED pattern of the same sample at 66 eV. Tunneling parameters are I_t = 1.36 nA and U_{bias} = −0.559 V for both images.

(resulting in a high intensity), while the others are aligned with respect to the center of the hexagons of the first plane (low or absent intensity).

In addition, the LEED pattern of this sample exhibits (1 × 1) Gr and (1 × 1) SiC intense spots, while (6 × 6) reconstruction is invisible (Figure 5c) confirming the absence of the buffer layer in agreement with STM observations.

XPS spectra of C 1s (Figure 6) recorded on this sample have been analyzed in the same conditions as reported above. The C

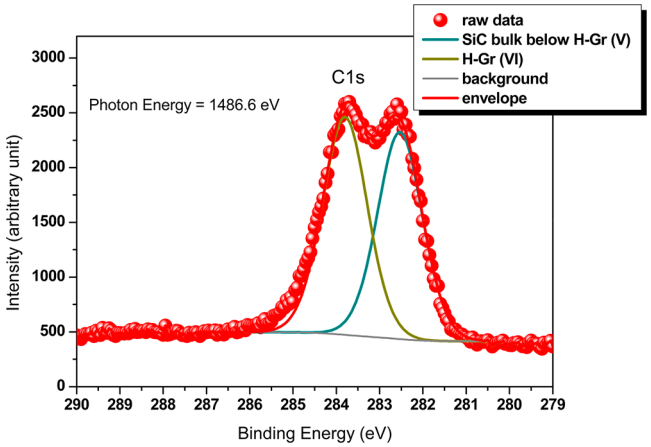

Figure 6. C 1s core level XPS spectrum of Gr grown with H_2 = 42% (sample C). The different fitted components (solid lines) are labeled in the spectrum. The solid red circles refer to the experimental data.

1s peak was deconvoluted assuming two components already identified in the literature for H-Gr:[65,66] (V) the Si−C component referring to the SiC bulk bonded to the hydrogen overlayer and (VI) the ML Gr with sp^2 configuration on hydrogen (decoupled from SiC underneath). The best fit is obtained when the C 1s experimental peak is deconvoluted into two components with E_{SiC} at 282.5 eV and E_{Gr} at 283.8 eV. A very small tail of the peak observed at high energy has already been observed and is well-fitted by replacing the Lorentzian profile by a Doniach−Sunjic profile in the pseudo-Voigt function.[41b] We can note that there is a large shift (0.9 eV) between the SiC signatures of this H-Gr sample and of the previous (6 × 6) Gr sample, with a lower binding energy when SiC is bound to H than when it is bound to the buffer layer (6 × 6) Gr. This was explained in the literature by different band bending occurring at the SiC substrate/Gr interface induced by different doping types between H-Gr (type P) and (6 × 6) Gr (type N).[45,61,64] It was also confirmed by ARPES.[25]

As above, we are concerned by the homogeneity and the thickness of the Gr film that are crucial for many potential applications. The number of deposited layers was evaluated as above, by the quantification of the C 1s/Si 2p area ratio. It is found for this sample around 1.1 which excludes the possibility for having more than 1 ML and attests the presence of a single H-Gr ML. This result is consistent with the STM images (reported above), which shows evidence for an equivalent intensity of the six atoms of the (1 × 1) Gr hexagonal cell as expected for the first free-standing H-Gr layer; otherwise, we should have seen a high-resolution STM arrangement like graphite.

STM, LEED, and XPS show that the use of a high H_2 flow rate ensures the production of H-Gr layers of very high quality, good homogeneity on a full-sample scale, and uniform ML thickness. They also show that by tuning the H_2 flow rate, we can switch from full hydrogenated Gr to (6 × 6) Gr completely free of hydrogen Gr, lying on the buffer layer, while keeping the layer homogeneous, flat, and uniform on the full-sample scale.

Let us turn now to the intermediate H_2/Ar ratios in between the two preceding situations. We have chosen to report the archetypal surface structure obtained for the H_2 ratio ∼33% (sample B in Table 1), but several samples with 10% < H_2 ratio <42% were performed which gave similar results though with different proportions of the observed configurations (see quantification and details of the procedure in Supporting Information S1). For sample B, STM observations reveal the juxtaposition of terraces with (6 × 6) Gr and H-Gr domains on large scales (Figure 7a) whose morphologies are similar to those reported above [sample A for (6 × 6) Gr terraces and sample C for H-Gr terraces]. In other words, in sample B, the size of the terraces is halved in comparison to the two other samples A and C (where the size of the terraces is similar to those of the SiC substrate terraces). The higher magnification images of the interface between these two domains (Figure 7b−d) give evidence for nonstraight step edges with nanofacets following armchair directions for the most part and associated to kinks of 2 nm length, well-matching the (6 × 6) unit cells (in size and direction). This observation suggests that the transformation from one configuration to another is made by hopping of the (6 × 6) unit cell following armchair directions. The LEED pattern of the sample (Figure 7c) is fully consistent with STM observations and confirms the presence of both configurations with intense Gr spots, surrounded by less intense diffraction spots of (6 × 6) Gr. This whole body of evidence proves that the sample is in a metastable (or pseudo-equilibrium) state with a transformation from the completely

https://doi.org/10.1021/acsanm.1c00082
ACS Appl. Nano Mater. 2021, 4, 4462−4473

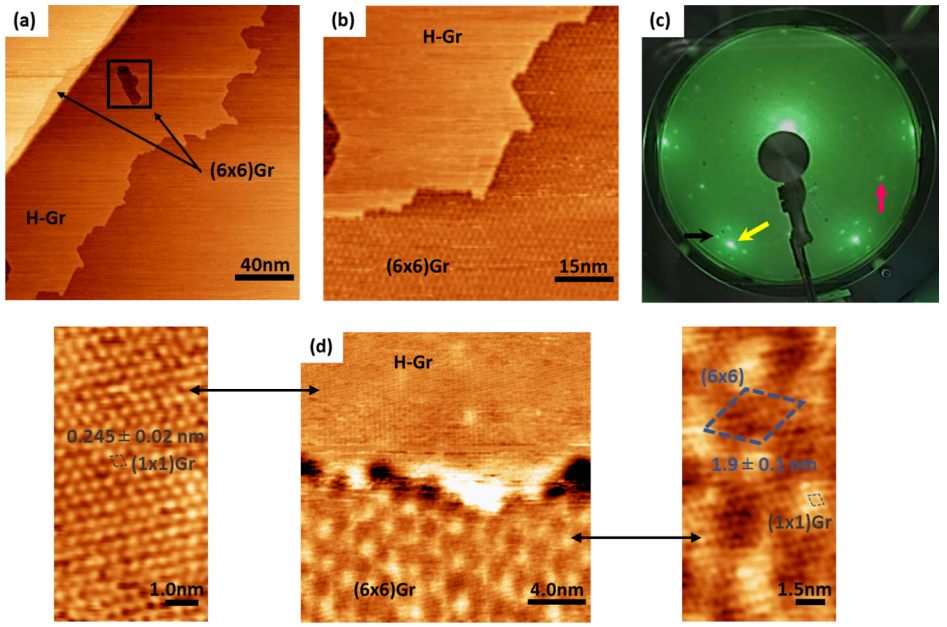

Figure 7. (a) Large-scale STM image of Gr grown with H_2 = 33% (sample B). (b) Higher magnification image of the interface between H-Gr and (6 × 6) Gr domains. (c) LEED pattern of the corresponding sample. Pink, yellow, and black arrows indicate (1 × 1) SiC, (1 × 1) Gr, and ($6\sqrt{3} \times 6\sqrt{3}$) Gr, respectively. (d) Atomic resolution image of the two configurations and their interface. The insets represent the atomic resolution of H-Gr (left) and (6 × 6) Gr (right). Tunneling parameters for (a,b) I_t = 0.317 nA U_{bias} = −0.856 V; (d) insets: I_t = 0.317 nA, U_{bias} = −0.456 V.

hydrogenated sample to the nonhydrogenated sample that can be tuned with the H_2 ratio. The distribution of the (6 × 6) Gr can be estimated from XPS spectra (Figure 8). In this sample, a

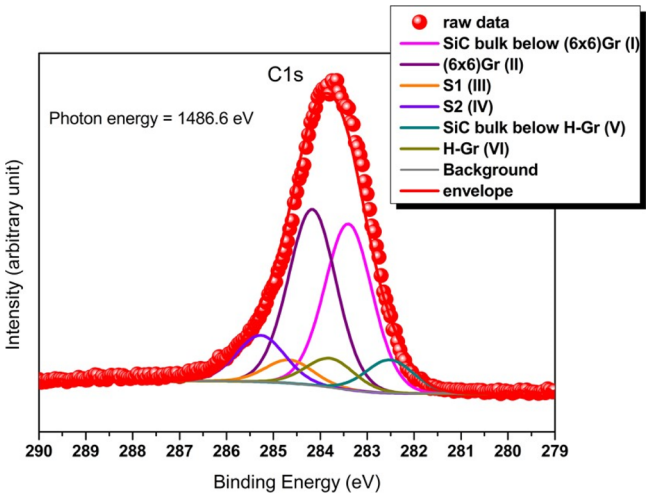

Figure 8. C 1s core level XPS spectrum of Gr grown with H_2 = 33% (sample B) and their deconvolution into different carbon components. The different fitted components (solid lines) are labeled in the spectrum. The solid red circles refer to the experimental data.

repartition of 15% H-Gr/85% (6 × 6) Gr has been estimated using the XPS procedure (Supporting Information S1). This is in good agreement with terrace repartition measured by STM, where a 65% coverage ratio was assessed for (6 × 6) Gr on large-scale images after identification at high resolution of the two domains. This large H-Gr/(6 × 6) Gr ratio explains the high intensity of the (6 × 6) patterns. It is worth mentioning that LEED does not provide quantitative information on the H-Gr/(6 × 6) Gr ratio since only the diffracting spots resulting from diffracting matter are visible. It is then not possible to distinguish by LEED full Gr on buffer and the partly hydrogenated Gr layer.

In summary, AFM observations of Gr/6H−SiC show that whatever the growth conditions are, the surface consists of wide terraces (some hundred nanometers large) separated by a regular train of tri-layer SiC steps (0.75 nm high) with accidently few ML steps (0.25 nm high multiple) or six-layer steps (1.5 nm high). It is obvious that AFM observations cannot visualize the single ML Gr which uniformly covers the SiC substrate with a carpet-like morphology. They neither discriminate the surface configurations between H-Gr (hydrogenated Gr) and (6 × 6) Gr (Gr on buffer layer) domains. In spite of this, we note that AFM is very often used to show the homogeneity of Gr thin films, in particular, to be processed in various devices or before deposition of further epitaxial layers, for example, for the growth of van der Waals heterostructures, whereas the Gr atomic structure has a strong influence on both the electronic properties of Gr and on the adsorption energy of many species and their subsequent growth mode.[67]

The developed CVD process, which involves a combination of complex processes based on the interaction of H_2/Ar and C_3H_8, is very robust and reliable. We have shown that it produces a uniform ML Gr on a full-sample scale, whose atomic properties [H-Gr or (6 × 6) Gr] can be varied at will, by tuning the H_2/Ar flow rate. This provides exceptional conditions to study the growth mechanism and the transition from one domain to another in detail. In addition, we have shown for the first time, that the proportions of H-Gr and (6 × 6) Gr can be realistically quantified on a large scale by XPS, using a detailed and precise procedure explained in Supporting Information. The quantifications obtained have been confirmed by STM assessments.

The growth process can be separated in three chronological stages: (i) sample heating, (ii) Gr growth, and (iii) sample cooling. During heating, three mechanisms are at work: Si and C sublimation, SiC etching, and passivation by hydrogen. Since

https://doi.org/10.1021/acsanm.1c00082
ACS Appl. Nano Mater. 2021, 4, 4462−4473

a large etching rate favors surface roughening, Ar is used to reduce SiC etching (part of the desorbed C and Si atoms collide with argon atoms and return to the surface). Associated to Ar, H_2 slowly etches and flattens the SiC surface, catalyzing C and Si atom sublimation accompanied by the formation of Si−H and C−H species. Simultaneously, it also fully covers and passivates the surface. The H_2/Ar ratio is then crucial to provide a flat and fully passivated surface during the heating stage. As a consequence, at the end of sample heating, when the growth temperature is reached (~1500−1600 °C), the SiC surface is fully covered by hydrogen. The high growth temperatures used help to restructure and uniformize the terrace morphology as explained above.

When the C_3H_8 carbon source is introduced in the gas mixture, etching stops, and quasi-equilibrium conditions are achieved between (i) etching/sublimation, (ii) H_2 adsorption, and (iii) C deposition. In these conditions, the growth is self-limited to a single ML of Gr even for longer deposition times. For large proportions of H_2, the surface remains fully hydrogenated through all the deposition duration, and a single ML of Gr uniformly covers the H-terminated SiC substrate leading to a single H-Gr domain which is well identified by STM observations that reveal only the Gr atomic cell. LEED and XPS analyses confirm the presence of only H-Gr at the sample scale.

When reducing the H_2 ratio, part of the hydrogen covering the substrate at the beginning of the growth starts to desorb during the deposition of carbon. The proportion of H-Gr decreases, and we observe the simultaneous presence of H-Gr and (6 × 6) Gr domains on juxtaposed terraces. To the best of our knowledge, such a morphology has never been observed before. In order to explain this behavior, we consider below the three hypotheses that may be at the origin of this morphology: (i) the simultaneous formation of the two domains; (ii) hydrogen intercalation below certain part of the (6 × 6) domain; (iii) partial desorption of H below the firstly nucleated H-Gr domain resulting in the formation of the (6 × 6) Gr. Thanks to the systematic observations of the domains and of their boundaries, we can rule out the two first hypotheses, and we claim that the (6 × 6) Gr domains are formed by the partial desorption of H.

This mechanism is supported by important aspects of the surface: first, the two juxtaposed domains have large sizes, whose boundaries follow the step edges; this is not compatible with hypothesis (i) where the concomitant formation of the two domains in a homogeneous atmosphere should result in small domains with arbitrary shapes. Second, we have demonstrated the presence of a single H-Gr ML. This is not consistent with hypothesis (ii) since the intercalation of H below the (6 × 6) Gr would produce two layers of Gr (as already reported in the literature). Third, several observations give evidence for the presence of (6 × 6) Gr areas fully surrounded by H-Gr domains (see Figure 6a for instance). Such a situation can only be explained by hypothesis (iii), where H desorbs from defects of hydrogenated Gr. We also observed the formation of (6 × 6) Gr along the step edges. This is also consistent with desorption of H from the step edges. After the desorption of hydrogen, the substrate rebuilds a buffer layer with (6 × 6) reconstruction for thermodynamic stability purposes (as already reported for epitaxial Gr obtained by SiC sublimation), and the Gr layer spontaneously transforms into (6 × 6) Gr.

In addition, we have shown that the step edges between the two domains [H-Gr and (6 × 6) Gr] have mostly armchair orientation, which is the predominant stable configuration and the signature of passivated H-Gr edges.[68]

The stability of the armchair step edge configuration in the presence of hydrogen was explained by both the lower energy of armchair edge (due to triple bonds in the "armrests" while zigzag edges end with strong and expensive dangling bonds) and the weak adsorption of H for armchair (4.36 eV) compared to zigzag (5.36 eV) which stems from the triple bonds in the armchair edge. This proves that in our experimental conditions, the step edges are hydrogenated. Finally, we have also observed that the step edges are composed of juxtaposition of the (6 × 6) kinks. This confirms that the transition from one domain to another occurs by hopping of a complete (6 × 6) unit cell, which is well consistent with the reconstruction of the substrate into (6 × 6) unit cells after the desorption of hydrogen.

As a consequence, we confirm that the (6 × 6) Gr results from the desorption of H-Gr when the H flow is reduced: at the end of the heating process, at the beginning of the C deposition, the substrate is completely covered by hydrogen. Gr nucleates directly on the hydrogenated substrate and eventually transforms (during the growth process) into (6 × 6) Gr after hydrogen desorption from step edges or defects on the terraces. A full confirmation of the proposed mechanism could be obtained by real-time monitoring of the surface during the different phases of the growth process.

When reducing further the H_2/Ar ratio, even if the substrate is fully covered by hydrogen, the formation of H-Gr is very unlikely: during the deposition of carbon, either H-Gr is totally inhibited or H-Gr is converted into (6 × 6) Gr by immediate H- desorption (due to the lack of H_2 molecules). At the end of the growth process, the surface exhibits a single (6 × 6) domain at the sample scale, which is well identified by the superimposition of the two structures [(6 × 6) reconstruction and Gr atomic cell] on STM images. LEED and XPS analyses also confirm the presence of a single (6 × 6) Gr domain. It is worth noting that during the cooling stage, the adsorption of hydrogen atoms from H_2 molecules is not favored due to the cost of the H_2 dissociation energy, unless the adsorption process should be even more complicated. In fact, the hypothesis of hydrogenation during cooling down was first considered. However, examining the STM images for various H_2 flows (we have taken hundreds of STM images, and we only presented some of them for three representative situations), we concluded that the hydrogenation of the Gr layer during the post-growth process (temperature drop) does not explain our observations. Indeed, it cannot be possible to have small areas of (6 × 6) Gr in the middle of the H-Gr terraces, if hydrogenation takes place during cooling down. It is really unlikely to have hydrogenation of complete terraces except from small areas surrounded by H-Gr areas at this stage.

CONCLUSIONS

By a combined study using a well-controlled growth process and systematic and careful analyses, we have identified the major steps of the complex Gr growth mechanism in the presence of H_2, Ar, and C_3H_8. For the first time, we have shown that the quasi-equilibrium growth process is self-limited and forms a single Gr layer independent of the growth duration. At the end of the heating stage, the substrate is fully covered by hydrogen. During carbon deposition, the first stage

https://doi.org/10.1021/acsanm.1c00082
ACS Appl. Nano Mater. 2021, 4, 4462−4473

is the direct growth of a fully hydrogenated Gr layer (H-Gr) over the total wafer scale. Depending on the H_2 flux, it eventually transforms into (6 × 6) Gr on the $(6\sqrt{3} \times 6\sqrt{3})$ R30° buffer layer by H-desorption from either step edges or defects on the terraces. When reducing the H_2 flow, such a CVD growth mechanism creates coexisting domains of the two surface structures, which are not distinguishable by AFM observations. It is also a unique process to produce whole layers of hydrogenated Gr (H-Gr) at high H_2 flow and of Gr on the buffer layer [(6 × 6) Gr] at low H_2 flow. It is worth noting that the step edges have an armchair configuration that could have major impacts, not only from the viewpoint of potential applications (since H-passivated armchair edges have strong influence on the electronic structure of Gr) but also for fundamental science. We also show a robust and generic procedure based on XPS data which allows us to realistically quantify the proportions of H-Gr and (6 × 6) Gr domains of a Gr film synthetized in any experimental conditions. Such proportions are of crucial importance for the electronic properties of the Gr layers and for the growth of subsequent layers on top of Gr. We have achieved a precise identification of new Gr surface structures, which provides the groundwork for the use of Gr as a template layer for van der Waals heteroepitaxy. The Gr/SiC heterojunctions fabricated here have unique uniformity fully compatible and suitable for microelectronic applications such as field effect transistors.

EXPERIMENTAL SECTION

Gr samples were grown on a Si-terminated face of nominally on-axis silicon carbide 6H−SiC(0001) by CVD in a hot wall horizontal growth chamber. The silicon carbide substrates (6H−SiC) are on-axis n-doped (nitrogen) 2″ wafers with a typical thickness of ∼350 μm from Tankeblue. Typical residual offcuts are between 0.05 and 0.2° toward the [1−100] direction, as deduced from AFM measurements on annealed substrates under H_2.[42] Before introduction into the growth chamber, the substrates are cut into 1 × 1 cm^2 pieces and then chemically cleaned with isopropanol. Gr deposition was carried out in a horizontal CVD reactor allowing a homogeneous and reproducible deposition of Gr on the substrates, at a pressure of 800 mbar s using a gas mixture of propane (C_3H_8) as the carbon source and hydrogen (H_2) and argon (Ar) as the carrier gases. The growth temperature was varied between 1550 and 1650 °C[42] and durations between 5 and 15 min. The H_2 flow ratio (H_2 flow/total flow) was varied between 9 and 42%. The propane flow ratio was 0.04 or 0.08%. During the temperature ramp to reach the growth temperature and during the cooling down, only the carrier gases (H_2 + Ar) were introduced into the growth chamber. Cooling down to room temperature begins at a rate about 4 °C/min.

In this study, we report the results obtained on three representative samples obtained with different H_2 flow ratios: (A) 9, (B) 33, and (C) 42%. The other experimental conditions listed in Table 1 are expected to have almost no influence on the Gr/substrate interactions as already reported.

Morphological characterization of the samples was investigated by near field microscopy: AFM in tapping mode in air using a silicon tip and scanning tunneling microscopy (STM) using electrochemically etched tungsten tips in UHV conditions. The UHV chamber was equipped with LEED, monochromatic X-ray photoemission spectroscopy (XPS), and STM (Omicron). STM observations were carried out at room temperature using constant current mode with I_t = 0.3 nA and V_t—between 0.4 and 1.5 V. A photon energy of 1486.6 eV (Al Kα) for XPS measurements was used for all the samples. The photoelectrons are analyzed with an Omicron EA 125 energy analyzer. The procedure for XPS quantitative analysis of C/Si is detailed in Supporting Information (S1). AFM and STM data were analyzed by WSxM[69] and ImageJ software. The XPS spectra were fitted using CasaXPS software. Cross-section TEM samples were prepared using a FEI Helios 600 Dual Beam Ga^+ focus ion beam. HRTEM observations were performed using a FEI Titan 80−300 Cs corrected microscope, operating at 200 keV.

ASSOCIATED CONTENT

Supporting Information

The Supporting Information is available free of charge at https://pubs.acs.org/doi/10.1021/acsanm.1c00082.

Description of the XPS quantitative analysis procedure and a large-scale TEM cross-sectional image (PDF)

AUTHOR INFORMATION

Corresponding Author

Isabelle Berbezier − *Aix Marseille University, Université de Toulon, CNRS, IM2NP, Marseille 13397, France;* orcid.org/0000-0003-1356-7527; Email: isabelle.berbezier@im2np.fr

Authors

Zouhour Ben Jabra − *Aix Marseille University, Université de Toulon, CNRS, IM2NP, Marseille 13397, France*

Adrien Michon − *CRHEA, Université Côte d'Azur, CNRS, Valbonne 06560, France*

Mathieu Koudia − *Aix Marseille University, Université de Toulon, CNRS, IM2NP, Marseille 13397, France*

Elie Assaf − *Aix Marseille University, Université de Toulon, CNRS, IM2NP, Marseille 13397, France*

Antoine Ronda − *Aix Marseille University, Université de Toulon, CNRS, IM2NP, Marseille 13397, France*

Paola Castrucci − *Dipartimento di Fisica, Università di Roma Tor Vergata, Roma 00133, Italy;* orcid.org/0000-0001-8986-7185

Maurizio De Crescenzi − *Dipartimento di Fisica, Università di Roma Tor Vergata, Roma 00133, Italy;* orcid.org/0000-0002-2935-8714

Holger Vach − *LPICM, CNRS, Ecole Polytechnique, IP Paris, Palaiseau 91128, France;* orcid.org/0000-0002-9359-2409

Mathieu Abel − *Aix Marseille University, Université de Toulon, CNRS, IM2NP, Marseille 13397, France*

Complete contact information is available at: https://pubs.acs.org/10.1021/acsanm.1c00082

Notes

The authors declare no competing financial interest.

ACKNOWLEDGMENTS

H.V. gratefully acknowledges the HPC centers of IDRIS (Grant A008-0900642) and CERMM for computational resources. P.C. and M.D.C. would like to acknowledge the European Community for the HORIZON2020 MSC-RISE Project DiSeTCom (GA 823728).

ADDITIONAL NOTES

[a]The $(6\sqrt{3} \times 6\sqrt{3})$ R30° supercell (with a periodicity of 3.2 nm) corresponds to the (6 × 6) Gr pseudo-supercell (with a periodicity of 1.9 ± 0.1 nm) for detailed description, see refs 61, 70. It also matches the (13 × 13) Gr supercell.

[b]Under our experimental conditions, there is almost no difference between asymmetric and symmetric fits (in line with the ∼0.1 eV XPS resolution). In the XPS results reported in literature, the asymmetric coefficient used is about 0.03, while

in our procedure, it should be lower than 0.005; in addition, it does not allow fitting the spectra correctly. In any case, the use of an asymmetric fit does not change the quantitative proportions of (6 × 6) Gr and H-Gr in the samples. For all these reasons, we preferred to use a symmetric function.

REFERENCES

(1) Novoselov, K. S.; Geim, A. K.; Morozov, S. V.; Jiang, D.; Zhang, Y.; Dubonos, S. V.; Grigorieva, I. V.; Firsov, A. A. Electric Field in Atomically Thin Carbon Films. *Science* **2004**, *306*, 666−669.

(2) Geim, A. K.; Novoselov, K. S. The Rise of Graphene. *Nat. Mater* **2007**, *6*, 183−191.

(3) Geim, A. K. Graphene: Status and Prospects. *Science* **2009**, *324*, 1530−1534.

(4) Novoselov, K. S. Nobel Lecture: Graphene: Materials in the Flatland. *Rev. Mod. Phys.* **2011**, *83*, 837−849.

(5) Tiwari, S. K.; Sahoo, S.; Wang, N.; Huczko, A. Graphene Research and Their Outputs: Status and Prospect. *J. Sci.: Adv. Mater. Devices* **2020**, *5*, 10−29.

(6) Zhou, S. Y.; Gweon, G.-H.; Fedorov, A. V.; First, P. N.; De Heer, W. A.; Lee, D.-H.; Guinea, F.; Castro Neto, A. H.; Lanzara, A. Substrate-Induced Bandgap Opening in Epitaxial Graphene. *Nature Mater* **2007**, *6*, 770−775.

(7) Emtsev, K. V.; Seyller, T.; Speck, F.; Ley, L.; Stojanov, P.; Riley, J. D.; Leckey, R. C. G. Initial Stages of the Graphite-SiC(0001) Interface Formation Studied by Photoelectron Spectroscopy. *Msf* **2007**, *556*−*557*, 525−528.

(8) Novoselov, K. S.; Geim, A. K.; Morozov, S. V.; Jiang, D.; Katsnelson, M. I.; Grigorieva, I. V.; Dubonos, S. V.; Firsov, A. A. Two-Dimensional Gas of Massless Dirac Fermions in Graphene. *Nature* **2005**, *438*, 197−200.

(9) Morozov, S. V.; Novoselov, K. S.; Katsnelson, M. I.; Schedin, F.; Elias, D. C.; Jaszczak, J. A.; Geim, A. K. Giant Intrinsic Carrier Mobilities in Graphene and Its Bilayer. *Phys. Rev. Lett.* **2008**, *100*, 11−14.

(10) Ni, Z. H.; Ponomarenko, L. A.; Nair, R. R.; Yang, R.; Anissimova, S.; Grigorieva, I. V.; Schedin, F.; Blake, P.; Shen, Z. X.; Hill, E. H.; Novoselov, K. S.; Geim, A. K. On Resonant Scatterers as a Factor Limiting Carrier Mobility in Graphene. *Nano Lett.* **2010**, *10*, 3868−3872.

(11) Usachov, D. Y.; Davydov, V. Y.; Levitskii, V. S.; Shevelev, V. O.; Marchenko, D.; Senkovskiy, B. V.; Vilkov, O. Y.; Rybkin, A. G.; Yashina, L. V.; Chulkov, E. V.; Sklyadneva, I. Y.; Heid, R.; Bohnen, K.-P.; Laubschat, C.; Vyalikh, D. V. Raman Spectroscopy of Lattice-Matched Graphene on Strongly Interacting Metal Surfaces. *ACS Nano* **2017**, *11*, 6336−6345.

(12) Nam, J.; Kim, D.-C.; Yun, H.; Shin, D. H.; Nam, S.; Lee, W. K.; Hwang, J. Y.; Lee, S. W.; Weman, H.; Kim, K. S. Chemical Vapor Deposition of Graphene on Platinum: Growth and Substrate Interaction. *Carbon* **2017**, *111*, 733−740.

(13) Silva, C. C.; Iannuzzi, M.; Duncan, D. A.; Ryan, P. T. P.; Clarke, K. T.; Küchle, J. T.; Cai, J.; Jolie, W.; Schlueter, C.; Lee, T.-L.; Busse, C. Valleys and Hills of Graphene on Ru(0001). *J. Phys. Chem. C* **2018**, *122*, 18554−18561.

(14) Mok, H. S.; Ebnonnasir, A.; Murata, Y.; Nie, S.; McCarty, K. F.; Ciobanu, C. V.; Kodambaka, S. Kinetics of Monolayer Graphene Growth by Segregation on Pd(111). *Appl. Phys. Lett.* **2014**, *104*, 101606.

(15) Wu, R.; Ding, Y.; Yu, K. M.; Zhou, K.; Zhu, Z.; Ou, X.; Zhang, Q.; Zhuang, M.; Li, W.-D.; Xu, Z.; Altman, M. S.; Luo, Z. Edge-Epitaxial Growth of Graphene on Cu with a Hydrogen-Free Approach. *Chem. Mater.* **2019**, *31*, 2555−2562.

(16) Koybasi, O.; Cazalas, E.; Childres, I.; Jovanovic, I.; Chen, Y. P. Detection of Light, X-Rays, and Gamma Rays Using Graphene Field Effect Transistors Fabricated on SiC, CdTe, and AlGaAs/GaAs Substrates. *2013 IEEE Nuclear Science Symposium and Medical Imaging Conference (2013 NSS/MIC)*; IEEE, 2013; pp 1−6.

(17) Britnell, L.; Gorbachev, R. V.; Jalil, R.; Belle, B. D.; Schedin, F.; Katsnelson, M. I.; Eaves, L.; Morozov, S. V.; Mayorov, A. S.; Peres, N. M. R.; Castro Neto, A. H.; Leist, J.; Geim, A. K.; Ponomarenko, L. A.; Novoselov, K. S. Electron Tunneling through Ultrathin Boron Nitride Crystalline Barriers. *Nano Lett.* **2012**, *12*, 1707−1710.

(18) Novoselov, K. S.; Fal'ko, V. I.; Colombo, L.; Gellert, P. R.; Schwab, M. G.; Kim, K. REVIEW A Roadmap for Graphene. *Nature* **2012**, *490*, 192−200.

(19) Kang, J.; Shin, D.; Bae, S.; Hong, B. H. Graphene Transfer: Key for Applications. *Nanoscale* **2012**, *4*, 5527−5537.

(20) Bonaccorso, F.; Lombardo, A.; Hasan, T.; Sun, Z.; Colombo, L.; Ferrari, A. C. Production and Processing of Graphene and 2d Crystals. *Mater. Today* **2012**, *15*, 564−589.

(21) Emtsev, K. V.; Bostwick, A.; Horn, K.; Jobst, J.; Kellogg, G. L.; Ley, L.; McChesney, J. L.; Ohta, T.; Reshanov, S. A.; Röhrl, J.; Rotenberg, E.; Schmid, A. K.; Waldmann, D.; Weber, H. B.; Seyller, T. Towards Wafer-Size Graphene Layers by Atmospheric Pressure Graphitization of Silicon Carbide. *Nature Mater* **2009**, *8*, 203−207.

(22) Avila, J.; Vignaud, D.; Godey, S.; Wallart, X.; Woodruff, D. P. Structural Determination of Bilayer Graphene on SiC (0001) Using Synchrotron Radiation Photoelectron Diffraction. *Sci. Rep.* **2018**, *8*, 10190.

(23) Charrier, A.; Coati, A.; Argunova, T.; Thibaudau, F.; Garreau, Y.; Pinchaux, R.; Forbeaux, I.; Debever, J.-M.; Sauvage-Simkin, M.; Themlin, J.-M. Solid-State Decomposition of Silicon Carbide for Growing Ultra-Thin Heteroepitaxial Graphite Films. *J. Appl. Phys.* **2002**, *92*, 2479−2484.

(24) Emtsev, K. V.; Speck, F.; Seyller, T.; Ley, L.; Riley, J. D. Interaction, Growth, and Ordering of Epitaxial Graphene on SiC{0001} Surfaces: A Comparative Photoelectron Spectroscopy Study. *Phys. Rev. B: Condens. Matter Mater. Phys.* **2008**, *77*, 1−10.

(25) Tokarczyk, M.; Kowalski, G.; Możdżonek, M.; Borysiuk, J.; Stępniewski, R.; Strupiński, W.; Ciepielewski, P.; Baranowski, J. M. Structural Investigations of Hydrogenated Epitaxial Graphene Grown on 4H-SiC (0001). *Appl. Phys. Lett.* **2013**, *103*, 241915.

(26) Varchon, F.; Mallet, P.; Magaud, L.; Veuillen, J. Y. Rotational Disorder in Few-Layer Graphene Films on 6H-SiC (000-1): A Scanning Tunneling Microscopy Study. *Phys. Rev. B: Condens. Matter Mater. Phys.* **2008**, *77*, 18−20.

(27) Tromp, R. M.; Hannon, J. B. Thermodynamics and Kinetics of Graphene Growth on SiC(0001). *Phys. Rev. Lett.* **2009**, *102*, 1−4.

(28) Ouerghi, A.; Silly, M. G.; Marangolo, M.; Mathieu, C.; Eddrief, M.; Picher, M.; Sirotti, F.; El Moussaoui, S.; Belkhou, R.; De Photonique, L.; Nanostructures, D.; De Nozay, R. Large-Area and High-Quality Epitaxial Graphene on Off -Axis SiC Wafers. *ACS Nano* **2012**, *6*, 6075−6082.

(29) Mishra, N.; Boeckl, J.; Motta, N.; Iacopi, F. Graphene Growth on Silicon Carbide: A Review. *Phys. Status Solidi A* **2016**, *213*, 2277−2289.

(30) Riedl, C.; Coletti, C.; Iwasaki, T.; Zakharov, A. A.; Starke, U. Quasi-Free-Standing Epitaxial Graphene on SiC Obtained by Hydrogen Intercalation. *Phys. Rev. Lett.* **2009**, *103*, 2−5.

(31) Drnec, J.; Vlaic, S.; Carlomagno, I.; Gonzalez, C. J.; Isern, H.; Carlà, F.; Fiala, R.; Rougemaille, N.; Coraux, J.; Felici, R. Surface Alloying upon Co Intercalation between Graphene and Ir(1 1 1). *Carbon* **2015**, *94*, 554−559.

(32) De Campos Ferreira, R. C.; De Lima, L. H.; Barreto, L.; Silva, C. C.; Landers, R.; De Siervo, A. Unraveling the Atomic Structure of Fe Intercalated under Graphene on Ir(111): A Multitechnique Approach. *Chem. Mater.* **2018**, *30*, 7201−7210.

(33) Park, Y.; Jung, D.; Hwang, H.-N.; Hwang, C.-C. Electronic Structure of the Au-Intercalated Graphene/Ni(111) Surface. *Current Applied Physics* **2019**, *19*, 215−218.

(34) Morawski, I.; Wang, Y.; Dawczak-Dębicki, H.; Stobiecki, F.; Lewandowski, M.; Nowicki, M. Determining the Structure of a Layer under 2D-Cover: The Case of Pb underneath Epitaxial Graphene on Ru(0001). *FlatChem* **2020**, *20*, 100158.

https://doi.org/10.1021/acsanm.1c00082
ACS Appl. Nano Mater. 2021, 4, 4462−4473

(35) Kovalenko, S. L.; Andryushechkin, B. V.; Eltsov, K. N. STM Study of Oxygen Intercalation at the Graphene/Ni(111) Interface. *Carbon* **2020**, *164*, 198−206.
(36) Wei, M.; Fu, Q.; Wu, H.; Dong, A.; Bao, X. Hydrogen Intercalation of Graphene and Boron Nitride Monolayers Grown on Pt(111). *Top. Catal.* **2016**, *59*, 543−549.
(37) Beshkova, M.; Hultman, L.; Yakimova, R. Device Applications of Epitaxial Graphene on Silicon Carbide. *Vacuum* **2016**, *128*, 186−197.
(38) Moreau, E.; Ferrer, F. J.; Vignaud, D.; Godey, S.; Wallart, X. Graphene Growth by Molecular Beam Epitaxy Using a Solid Carbon Source. *phys. stat. sol. (a)* **2010**, *207*, 300−303.
(39) Strupinski, W.; Grodecki, K.; Wysmolek, A.; Stepniewski, R.; Szkopek, T.; Gaskell, P. E.; Grüneis, A.; Haberer, D.; Bozek, R.; Krupka, J.; Baranowski, J. M. Graphene Epitaxy by Chemical Vapor Deposition on SiC. *Nano Lett.* **2011**, *11*, 1786−1791.
(40) Portail, M.; Michon, A.; Vézian, S.; Lefebvre, D.; Chenot, S.; Roudon, E.; Zielinski, M.; Chassagne, T.; Tiberj, A.; Camassel, J.; Cordier, Y. Growth Mode and Electric Properties of Graphene and Graphitic Phase Grown by Argon − Propane Assisted CVD on 3C − SiC / Si and 6H − SiC. *Journal of Crystal Growth* **2012**, *349*, 27−35.
(41) Michon, A.; Vézian, S.; Ouerghi, A.; Zielinski, M.; Chassagne, T.; Portail, M. Direct Growth of Few-Layer Graphene on 6H-SiC and 3C-SiC/Si via Propane Chemical Vapor Deposition. *Appl. Phys. Lett.* **2010**, *97*, 2012−2015.
(42) Michon, A.; Vézian, S.; Roudon, E.; Lefebvre, D.; Zielinski, M.; Chassagne, T.; Portail, M. Effects of Pressure, Temperature, and Hydrogen during Graphene Growth on SiC(0001) Using Propane-Hydrogen Chemical Vapor Deposition. *J. Appl. Phys.* **2013**, *113*, 203501.
(43) Riedl, C.; Zakharov, A. A.; Starke, U.; Riedl, C.; Zakharov, A. A.; Starke, U. Precise in Situ Thickness Analysis of Epitaxial Graphene Layers on SiC (0001) Using Low-Energy Electron Diffraction and Angle Resolved Ultraviolet Photoelectron Spectroscopy. *Appl. Phys. Lett.* **2008**, *93*, 033106.
(44) Bueno, R. A.; Palacio, I.; Munuera, C.; Aballe, L.; Foerster, M.; Strupinski, W.; García-Hernández, M.; Martín-Gago, J. A.; López, M. F. Structural Characterization of As-Grown and Quasi-Free Standing Graphene Layers on SiC. *Appl. Surf. Sci.* **2019**, *466*, 51−58.
(45) Speck, F.; Jobst, J.; Fromm, F.; Ostler, M.; Waldmann, D.; Hundhausen, M.; Weber, H. B.; Seyller, T. The Quasi-Free-Standing Nature of Graphene on H-Saturated SiC(0001). *Appl. Phys. Lett.* **2011**, *99*, 7−10.
(46) Azizi, A.; Eichfeld, S.; Geschwind, G.; Zhang, K.; Jiang, B.; Mukherjee, D.; Hossain, L.; Piasecki, A. F.; Kabius, B.; Robinson, J. A.; Alem, N. Freestanding van Der Waals Heterostructures of Graphene and Transition Metal Dichalcogenides. *ACS Nano* **2015**, *9*, 4882−4890.
(47) Pierucci, D.; Henck, H.; Naylor, C. H.; Sediri, H.; Lhuillier, E.; Balan, A.; Rault, J. E.; Dappe, Y. J.; Bertran, F.; Le Fèvre, P.; Johnson, A. T. C.; Ouerghi, A. Large Area Molybdenum Disulphide- Epitaxial Graphene Vertical Van Der Waals Heterostructures. *Sci. Rep.* **2016**, *6*, 1−10.
(48) Li, G.; Zhang, L.; Xu, W.; Pan, J.; Song, S.; Zhang, Y.; Zhou, H.; Wang, Y.; Bao, L.; Zhang, Y.; Du, S.; Ouyang, M.; Pantelides, S. T.; Gao, H. Stable Silicene in Graphene/Silicene Van Der Waals Heterostructures. **2018**, *30*, 1804650. DOI: 10.1002/adma.201804650
(49) Yu, C.; He, Z. Z.; Song, X. B.; Liu, Q. B.; Han, T. T.; Dun, S. B.; Wang, J. J.; Zhou, C. J.; Guo, J. C.; Lv, Y. J.; Feng, Z. H.; Cai, S. J. Improvement of the Frequency Characteristics of Graphene Field-Effect Transistors on SiC Substrate. *IEEE Electron Device Lett.* **2017**, *38*, 1339−1342.
(50) Zhang, F.; Chen, X.; Yu, C.; Xu, X.; Hu, X.; Qin, X.; Li, Q.; Zhao, X.; Yu, P.; Wang, R. High Mobility and Large Domain Decoupled Epitaxial Graphene on SiC (0001) Surface Obtained by Nearly Balanced Hydrogen Etching. *Mater. Lett.* **2017**, *195*, 82−85.
(51) Sonde, S.; Giannazzo, F.; Vecchio, C.; Yakimova, R.; Rimini, E.; Raineri, V. Role of Graphene/Substrate Interface on the Local Transport Properties of the Two-Dimensional Electron Gas. *Appl. Phys. Lett.* **2010**, *97*, 138−141.
(52) Jabakhanji, B.; Michon, A.; Consejo, C.; Desrat, W.; Portail, M.; Tiberj, A.; Paillet, M.; Zahab, A.; Cheynis, F.; Lafont, F.; Schopfer, F.; Poirier, W.; Bertran, F.; Le Fèvre, P.; Taleb-Ibrahimi, A.; Kazazis, D.; Escoffier, W.; Camargo, B. C.; Kopelevich, Y.; Camassel, J.; Jouault, B. Tuning the Transport Properties of Graphene Films Grown by CVD on SiC(0001): Effect of in Situ Hydrogenation and Annealing. *Phys. Rev. B: Condens. Matter Mater. Phys.* **2014**, *89*, 085422.
(53) Dagher, R.; Blanquet, E.; Chatillon, C.; Journot, T.; Portail, M.; Nguyen, L.; Cordier, Y.; Michon, A. A Comparative Study of Graphene Growth on SiC by Hydrogen-CVD or Si Sublimation through Thermodynamic Simulations. *CrystEngComm* **2018**, *20*, 3702−3710.
(54) Michon, A.; Largeau, L.; Mauguin, O.; Ouerghi, A.; Vézian, S.; Lefebvre, D.; Roudon, E.; Zielinski, M.; Chassagne, T.; Portail, M. Graphene Growth Using Propane-Hydrogen CVD on 6H-SiC(0001): Temperature Dependent Interface and Strain. *Phys. Status Solidi C* **2012**, *9*, 175−178.
(55) Mallet, P.; Varchon, F.; Naud, C.; Magaud, L.; Berger, C.; Veuillen, J. Y. Electron States of Mono- and Bilayer Graphene on SiC Probed by Scanning-Tunneling Microscopy. *Phys. Rev. B: Condens. Matter Mater. Phys.* **2007**, *76*, 2−5.
(56) Kim, S.; Ihm, J.; Choi, H. J.; Son, Y. W. Origin of Anomalous Electronic Structures of Epitaxial Graphene on Silicon Carbide. *Phys. Rev. Lett.* **2008**, *100*, 2−5.
(57) Varchon, F.; Mallet, P.; Veuillen, J. Y.; Magaud, L. Ripples in Epitaxial Graphene on the Si-Terminated SiC(0001) Surface. *Phys. Rev. B: Condens. Matter Mater. Phys.* **2008**, *77*, 1−8.
(58) Huang, H.; Chen, W.; Chen, S.; Wee, A. T. S.; Wee, S. Bottom-up Growth of Epitaxial. *ACS Nano* **2008**, *2*, 2513−2518.
(59) Riedl, C.; Starke, U.; Bernhardt, J.; Franke, M.; Heinz, K. Structural Properties of the Graphene-SiC(0001) Interface as a Key for the Preparation of Homogeneous Large-Terrace Graphene Surfaces. *Phys. Rev. B: Condens. Matter Mater. Phys.* **2007**, *76*, 1−8.
(60) Brar, V. W.; Zhang, Y.; Yayon, Y.; Ohta, T.; McChesney, J. L.; Bostwick, A.; Rotenberg, E.; Horn, K.; Crommie, M. F. Scanning Tunneling Spectroscopy of Inhomogeneous Electronic Structure in Monolayer and Bilayer Graphene on SiC. *Appl. Phys. Lett.* **2007**, *91*, 1−4.
(61) Riedl, C.; Coletti, C.; Starke, U. Structural and Electronic Properties of Epitaxial Graphene on SiC(0001): A Review of Growth, Characterization, Transfer Doping and Hydrogen Intercalation. *J. Phys. D: Appl. Phys.* **2010**, *43*, 374009.
(62) Veuillen, J.-Y.; Hiebel, F.; Magaud, L.; Mallet, P.; Varchon, F. Interface Structure of Graphene on Sic: An Ab Initio and STM Approach. *J. Phys. D: Appl. Phys.* **2010**, *43*, 374008.
(63) Choi, J.; Lee, H.; Kim, S. Atomic-Scale Investigation of Epitaxial Graphene Grown on 6H-SiC(0001) Using Scanning Tunneling Microscopy and Spectroscopy. *J. Phys. Chem. C* **2010**, *114*, 13344−13348.
(64) Mammadov, S.; Ristein, J.; Koch, R. J.; Ostler, M.; Raidel, C.; Wanke, M.; Vasiliauskas, R.; Yakimova, R.; Seyller, T. Polarization Doping of Graphene on Silicon Carbide. *2D Mater.* **2014**, *1*, 035003.
(65) Sforzini, J.; Nemec, L.; Denig, T.; Stadtmüller, B.; Lee, T. L.; Kumpf, C.; Soubatch, S.; Starke, U.; Rinke, P.; Blum, V.; Bocquet, F. C.; Tautz, F. S. Approaching Truly Freestanding Graphene: The Structure of Hydrogen-Intercalated Graphene on 6h-Sic (0001). *Phys. Rev. Lett.* **2015**, *114*, 1−6.
(66) Yu, C.; Chen, X.; Zhang, F.; Sun, L.; Li, T.; Xu, X.; Zhao, X. Uniform Coverage of Quasi-Free Standing Monolayer Graphene on SiC by Hydrogen Intercalation. *J Mater Sci: Mater Electron* **2017**, *28*, 3884−3890.
(67) Sokolova, A.; Kilchert, F.; Link, S.; Stöhr, A.; Starke, U.; Schneider, M. A. Sub-Monolayer Growth of Titanium, Cobalt, and Palladium on Epitaxial Graphene. *Ann. Phys.* **2017**, *529*, 2−7.
(68) Koskinen, P.; Malola, S.; Häkkinen, H. Self-Passivating Edge Reconstructions of Graphene. *Phys. Rev. Lett.* **2008**, *101*, 2−5.

https://doi.org/10.1021/acsanm.1c00082
ACS Appl. Nano Mater. 2021, 4, 4462−4473

(69) Horcas, I.; Fernández, R.; Gómez-Rodríguez, J. M.; Colchero, J.; Gómez-Herrero, J.; Baro, A. M. WSXM: A Software for Scanning Probe Microscopy and a Tool for Nanotechnology. *Rev. Sci. Instrum.* **2007**, *78*, 013705.
(70) Ni, Z. H.; Chen, W.; Fan, X. F.; Kuo, J. L.; Yu, T.; Wee, A. T. S.; Shen, Z. X. Raman Spectroscopy of Epitaxial Graphene on a SiC Substrate. *Phys. Rev. B: Condens. Matter Mater. Phys.* **2008**, *77*, 1−6.

https://doi.org/10.1021/acsanm.1c00082
ACS Appl. Nano Mater. 2021, 4, 4462−4473